Colloidal nanocrystals for telecommunications. Complete coverage of the low-loss fiber windows by mercury telluride quantum dots*

M. T. Harrison[1†], S. V. Kershaw[1], M. G. Burt[1], A. L. Rogach[2‡], A. Kornowski[2], A. Eychmüller[2], and H. Weller[2]

[1]*Advanced Telecommunications Research, BT Adastral Park, Martlesham Heath, Ipswich, IP5 3RE, UK;* [2]*Institut für Physikalische Chemie, Universität Hamburg, 20146 Hamburg, Germany*

Abstract: Optical fibers have revolutionized the telecommunications industry to such an extent that the network capacity available today was unthinkable 20 years ago. Even so, with the advent of the datawave, and the exponential increase of network traffic predicted to continue indefinitely, the generation of bandwidth remains a challenge. One of the major limitations to the implementation of future high-capacity, ultra-broadband optical networks is the expansion of the fiber bandwidth beyond that available from the current state-of-the-art signal amplification device—the erbium-doped fiber amplifier (EDFA). Although there is currently a large effort to expand the flat-gain bandwidth of the EDFA, most of these efforts involve sophisticated engineering, exotic glass fibers, or multicomponent cascaded systems. In a radically different approach, we are attempting to use the unique properties of semiconductor nanocrystals, or quantum dots, as "designer atoms" in order to produce an ultra-broadband optical amplifier with complete coverage of the telecommunications wavelengths. In this paper we review the synthesis of thiol-stabilized mercury chalcogenide nanocrystals via an aqueous colloidal route, which demonstrate extremely intense photoluminescence all the way across the spectral region of interest, i.e., from 1000 to over 1700 nm.

INTRODUCTION

The telecommunications industry is currently facing a revolution. The recent explosion in non-voice traffic, fuelled mainly by the spectacular rise of the Internet, has exposed the need for improvements in network infrastructure. With Internet traffic growing at between 200 and 400% annually [1], traditional voice traffic is predicted to account for only 1% of the total traffic within about 5 years (compared with 50% today). Total network traffic is expected to be tens or even hundreds of terabits/s, and this burgeoning demand for high volume and high bit rate communications necessitates manipulation of the traffic in the optical domain as much as possible. As an introduction to optical fiber transmission, I will describe the origin of the strategically important 1300 and 1550 nm low-loss telecoms windows, the concept of wavelength divisional multiplexing (WDM), and their relationship to the erbium-doped fiber amplifier (EDFA), which has severe limitations for high-capacity optical transmission. I will then describe our recent work on mercury telluride quantum dots, and how this powerful, versatile, and low-cost materials technology could revolutionize the design of hardware for future broadband networks.
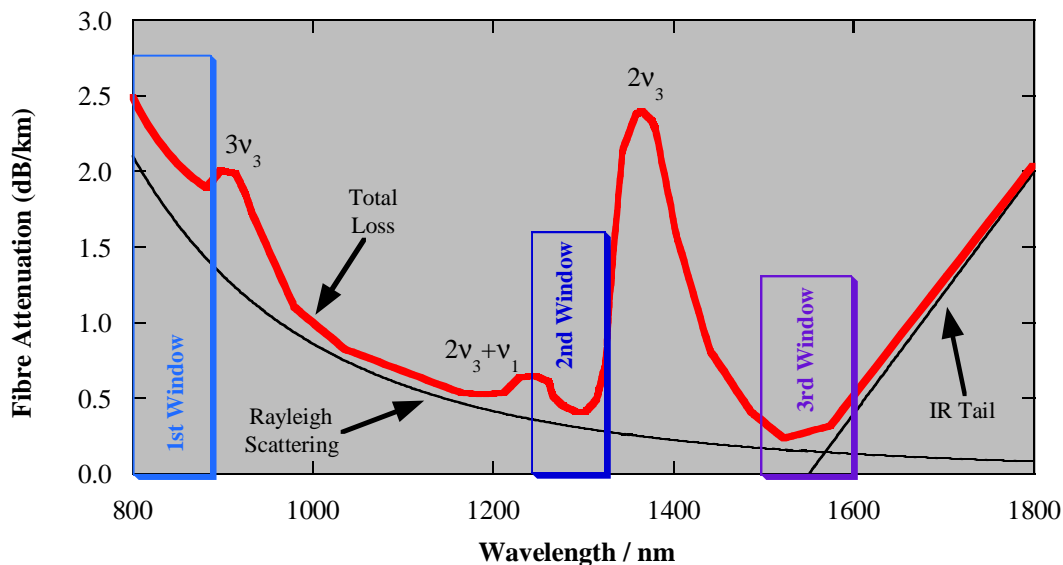
Fig. 1 Attenuation vs. wavelength curve for a standard silica optical fiber.

Optical fiber transmission

Figure 1 shows a typical attenuation vs. wavelength curve for a standard silica telecommunication optical fiber. The optical attenuation which occurs as a light beam passes through a transparent medium is due to a variety of mechanisms that are a function of the light wavelength. Transparency at longer wavelengths is limited by the infrared vibrational, or multiphonon, absorption edge, which is determined by the frequency of the fundamental lattice vibration. The other major intrinsic loss mechanism is Rayleigh scattering, which is caused by inhomogeneities of the dielectric constant on a scale much smaller than the wavelength of light [2]. The position and magnitude of the *theoretical* minimum loss is therefore determined by the intersection of these two curves [3]. However, in standard optical fiber the presence a few parts per billion of bound hydroxyl (SiOH) produces the various OH overtone and combination absorption bands which yield the so-called first, second, and third *low-loss optical fiber windows* around 850 nm, 1300 nm and 1550 nm respectively [4]. Therefore, the potentially huge bandwidth of the optical fiber for long-distance transmission is currently limited to two approximately 100 nm wide windows around 1300 nm and 1550 nm (the attenuation in the first window being too high).

However, the recent development of "water-free" AllWave™ single-mode optical fiber by Lucent Technologies [5] has opened up the entire 1280 to 1625 nm wavelength region. A new manufacturing process has virtually eliminated the incorporation of hydroxyl moieties and produced a fiber with close to the predicted theoretical minimum loss. Without the kind of restrictions caused by standard 'wet' fiber, the full bandwidth of tens of terahertz of optical fiber becomes available.

Wavelength divisional multiplexing (WDM)

One of the techniques that can exploit the massive bandwidth available from optical fiber transmission is wavelength divisional multiplexing (WDM) (Fig. 2a). At a very basic level this is simply the use of many different wavelengths, or channels, down the same fiber rather than a single wavelength (e.g.,
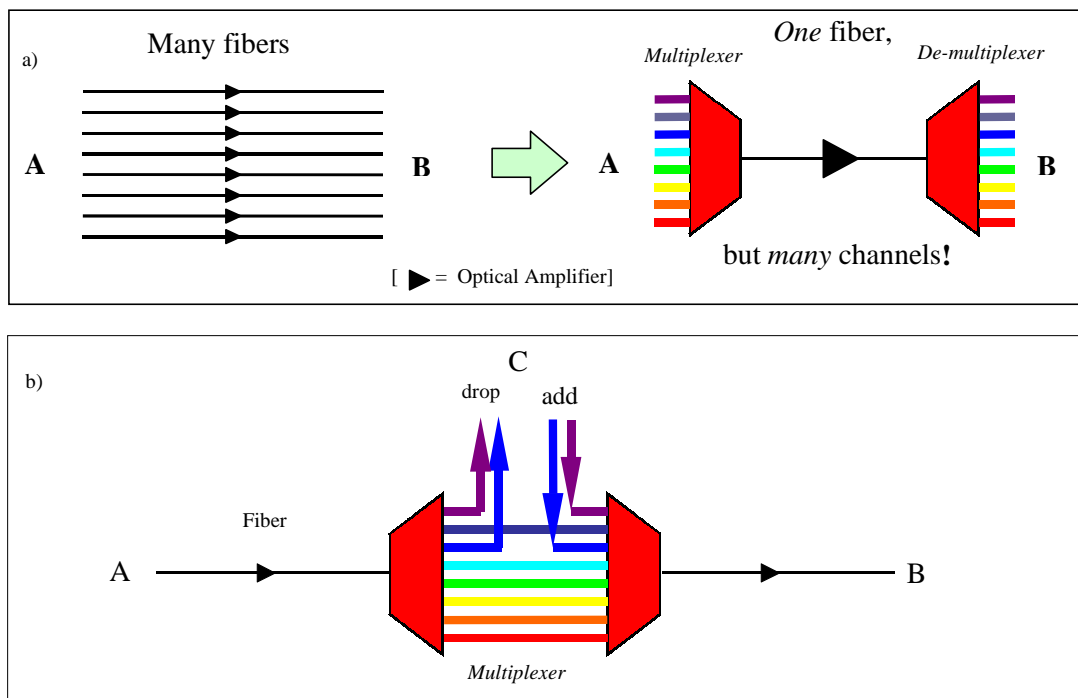
Fig. 2 Schematic diagrams of (a) point-to-point WDM, and (b) wavelength-dependent optical add/drop multiplexer (OADM).

8 channels at 2.5 gigabits/s gives a total data rate of 20 gigabits/s). It is a technique that can therefore use the full capacity of the installed fibers before having to dig up the roads to add more. Its other advantages and properties include: simple, passive multiplexing/demultiplexing; required receiver bandwidth is only tributary bandwidth; bit rate transparency and flexibility; fewer components (e.g., amplifiers); and the wavelength itself can be used as a parameter for switching and routing operations by the use of optical gratings and filters (Fig. 2b). Of critical importance in WDM systems is the channel spacing—too large and stimulated Raman scattering can lead to cross-talk; too small and four-wave mixing can give problems as well as much harder and more expensive multiplexing/demultiplexing, switching, and routing.

Erbium-doped fiber amplifiers (EDFAs)

Despite the attenuation in optical fibers being extremely low, when the transmission is over tens of kilometers, the signal does need to be periodically re-amplified. In the vitally important 1500 nm to 1600 nm 3rd telecoms window the current state-of-the-art device is the EDFA [6–8]. This device is an all-optical amplifier that exploits the single-pass gain available from the population inversion established optical pumping of a length of erbium-doped optical fiber (Fig. 3).

However, the EDFA has severe limitations for its use in high-capacity WDM systems, as can be seen in Fig. 4. The typical gain spectrum only covers around 30 nm of the 100 nm wide fiber window, and across this range requires external gain flattening to prevent unequal amplification of the different wavelengths. Therefore, any WDM architecture that requires optical amplifiers in the 1550 nm window is limited to squeezing the channels into this narrow bandwidth.
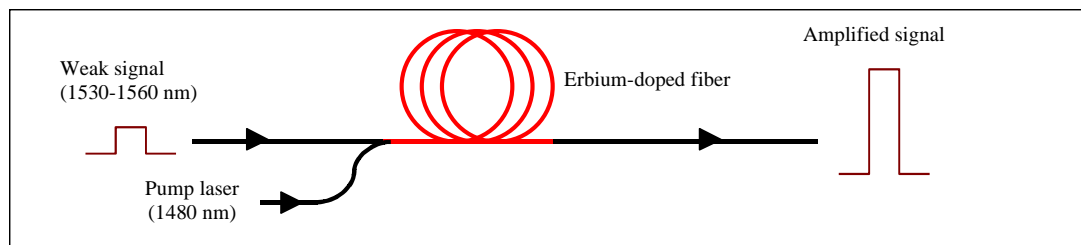
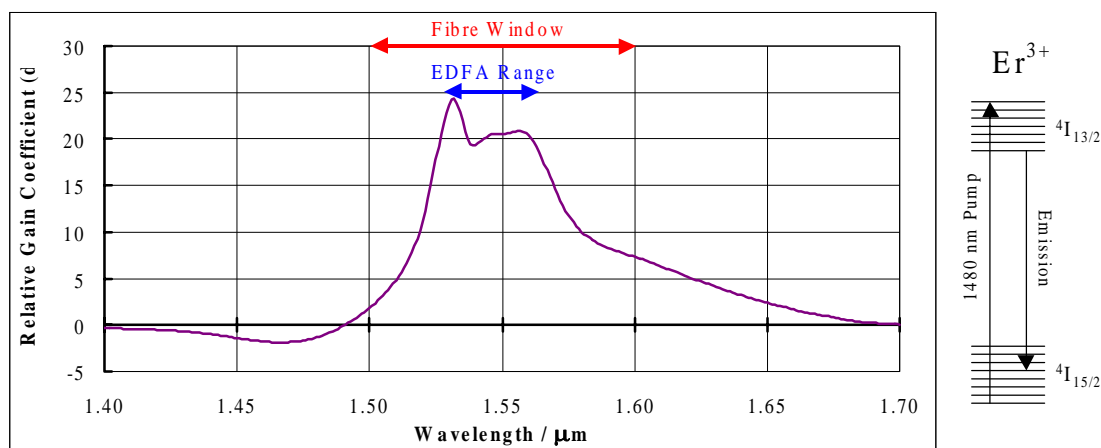**Fig. 3** Schematic diagram of a forward-pumped erbium-doped fiber amplifier.

Fig. 4 Typical gain spectrum for an EDFA (70% inversion). Also shown is the Er^{3+} gain transition using a 1480 nm pump.

Quantum dots and optical amplifiers

According to the 1998 Roadmap Report by the Optoelectronic Industry Development Association (OIDA), one of the key short- to mid-term component technologies for high-speed and broadband information is very low-cost and ultra-wideband optical amplifiers [1]. The shortcomings of the current EDFA technology, which does not even cover the full 1550 nm 3rd telecoms low-loss window in standard fiber, never mind the massive bandwidth of water-free fiber, means that an alternative is desperately required.

A great deal of work is being put into extending the range of the EDFA, either by optimizing the 1570 to 1610 nm (or 'L' band) long wavelength side of the gain profile, or by using different glass hosts with intrinsically broad gain spectra [8–10]. This technique often requires the cascading of several different amplifiers to only extend the gain width to 80 nm, and is therefore quite an expensive and complex approach. It is also possible to use different rare-earth (RE) ions for different parts of the spectrum (e.g., Pr^{3+} in fluoride glass has been tried for amplification in the 1300 nm 2nd telecoms window [11]), but these also suffer from the same problems as the EDFA. There are other alternatives to RE-doped glasses, such as Raman amplifiers [12–14] and optical paramagnetic amplifiers [15], but each of these technologies has its own drawbacks, such as high pump powers, availability of pump wavelengths, and limited bandwidth. It is clear that a radically different approach is required in order to achieve uniform amplification over the low-loss optical windows in both standard and water-free fibers.

The radically different approach we have taken is to use colloidal semiconductor nanocrystals, or quantum dots, as "artificial atoms", where the quantum confinement effect yields size-dependent opti-

cal properties. For a given material, therefore, the spectral width, position, and profile can be tailored to requirements by controlling the size distribution. It should therefore be possible to fill all the telecoms windows with flat gain and produce a true ultra-broadband optical amplifier, providing a suitable infra-red-emitting material can be found.

INFRARED COLLOIDAL QUANTUM DOTS

When the diameter of a semiconductor particle is comparable to, or less than, the exciton diameter in the bulk material, the bandgap energy is critically dependent on the size of the nanocrystal [16–18]. This so-called quantum confinement effect can be observed optically by a blue-shift in the photoluminescence energy from the bulk value, as well as a well-developed maxima near the absorption onset, which may be ascribed to the first excitonic transition. The size-dependent bandgap energy can be modelled using simple effective mass theories on particles in a 3D box [19–21]. Using this method, it is possible to predict which materials might operate at the telecoms wavelengths of interest. Figure 5 shows the positions of the bulk bandgap and bandgap energies at 3 nm and 10 nm particle sizes, calculated using the Masumoto and Sonobe model [21], for a selection of II-VI and III-V semiconductors. Energies corresponding to 1.3 and 1.550 µm are shown for reference to telecoms applications. The figure shows that the systems of interest may include GaSb, HgSe, HgTe, InAs, InSb, PbS, PbSe, and PbTe.

There are many different synthetic routes that may be used to form colloidal nanocrystals from the materials shown in Fig. 5. Apart from the relative simplicity of the syntheses, the colloidal route also offers an incredibly versatile and sophisticated technique with a large degree of control over the size and structure of the quantum dots. Organic surfactant molecules are used for passivation and size distribution, and many II-VI and III-V compounds can be formed using the "TOP/TOPO route" [22,23]. A
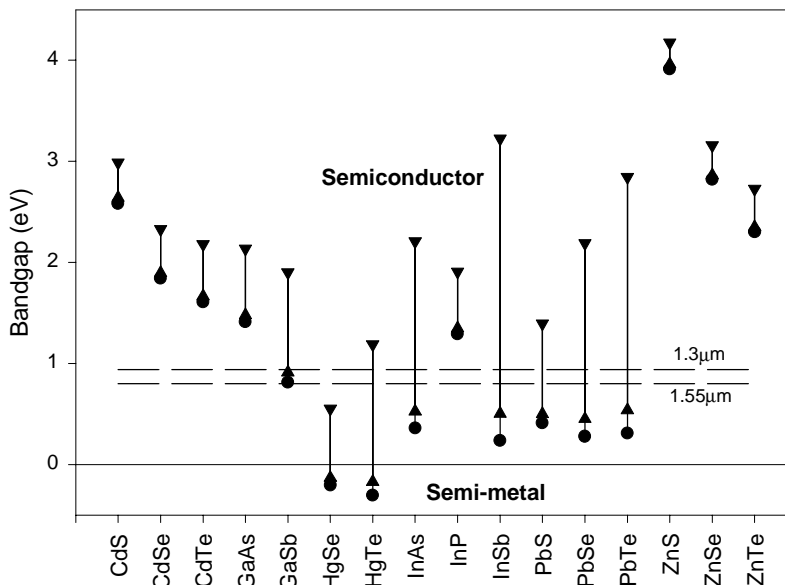

Fig. 5 Sensitivity of bandgap energies (calculated) to particle size for a range of semiconductors. Bandgaps are shown for the bulk forms (circles) and at a dot radii of 10 nm (up triangles) and 3 nm (down triangles).

metal alkyl reacts with a metal chloride (III-Vs) or TOP-chalcogenide (II-VIs) in a hot mixture of tri-octyl phosphine (TOP) and tri-octyl phosphine oxide (TOPO) with the mixture functioning as both solvent and stabilizing ligand. A low-temperature alternative to this for the more ionic II-VI nanocrystals is to use polar, aqueous solutions with, for example, thiols as the stabilizer [24–27]. It is also possible to form complex core-shell (e.g., CdSe/ZnS [28]), and quantum dot quantum well (e.g., CdS/HgS/CdS [29]) structures using these methods, adding to the degrees of freedom for their optical and physical properties.

Our initial attempts centered on InAs (TOP/TOPO) [30] and CdTe/HgTe/CdTe (aq) QDQWs [31] which had already been demonstrated to have infrared photoluminescence (PL), albeit at the short wavelength end of the telecoms region of interest. The extremely high quantum efficiency (QE) of the PL and some preliminary gain measurements from the telluride material prompted us to look at this system further.

CdTe/HgTe composite nanocrystals

In CdS/HgS-layered composites, the PL is red-shifted with respect to the bare CdS nanocrystals. Therefore, by starting with CdTe, which has a PL ~550 nm, layering with HgTe to form a QDQW should produce near-infrared emission. In order to investigate the full range of heterostructures, both core-shell CdTe/HgTe and QDQW CdTe/HgTe/CdTe were attempted, and the full range of syntheses has been described elsewhere [32]. We began with an aqueous solution of well-characterized 3-mercapto-1,2-propanediol (1-thioglycerol) stabilized CdTe with a narrow size distribution and a diameter ~2.4 nm [24]. Step 1 was then the addition of Hg^{2+} ions, which substitute for Cd^{2+} ions at the surface of the dot due to their solubility differences [29], to form a "locking" monolayer of HgTe (CdHgTe). The QDQW is formed by the precipitation of a layer of CdTe on the surface by addition of more Cd^{2+} ions and thioglycerol, then bubbling H_2Te gas through the solution (CdHgCdTe). Finally, in step 3 the substitution process was repeated to form, in theory, a "core/double-shell" CdHgHgTe compound. Figure 6 shows the absorption and room temperature PL spectra of the series CdTe, CdHgTe, CdHgCdTe, and CdHgHgTe.
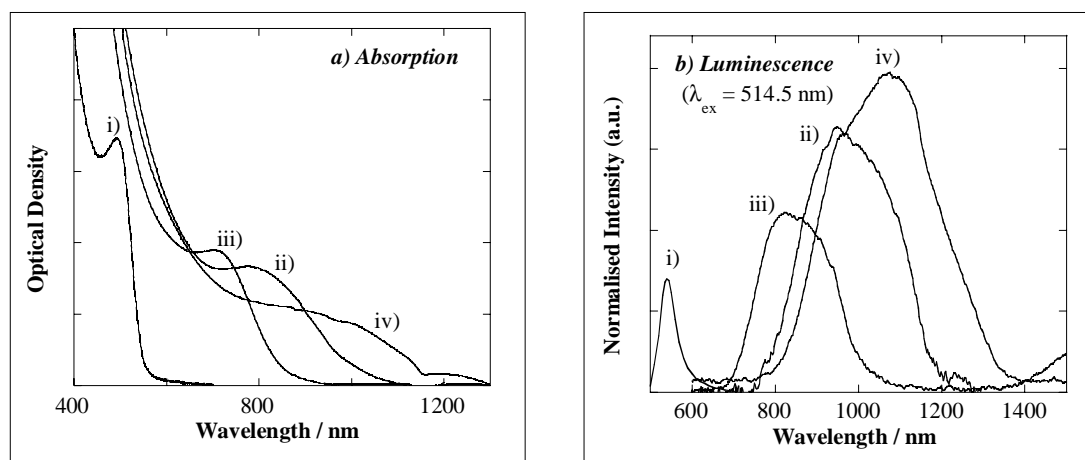

Fig. 6 (a) Absorption and (b) room-temperature photoluminescence spectra for (i) CdTe, (ii) CdHgTe, (iii) CdHgCdTe, and (iv) CdHgHgTe.

However, the series of spectra shown in Fig. 6 suggest that a $Cd_{1-x}Hg_xTe$ alloy is being formed rather than the discretely layered materials we had hoped for. For a layered compound the QDQW structure should have a small red-shift (or none at all) in the PL with respect to the core-shell precursor, not the observed blue-shift. In fact, the optical properties appear to be compositionally dependent, with the bandgap energy decreasing with increasing mercury content, up to limiting values of around 1100 nm and 50% for the PL wavelength and QE respectively. Therefore, in line with the predictions of Fig. 5, pure HgTe nanocrystals ($x = 1$) should possess our required infrared PL, and should be relatively easy to prepare.

HgTe nanocrystals

Bulk HgTe is a semi-metal with a small negative bandgap ($\Gamma_{6c} - \Gamma_{8v} = -0.3$) at room temperature [33]. Quantum confinement will add a positive term to this, which will increase as the particle size decreases, giving a potentially huge infrared tuning range for such materials (see Fig. 5). Colloidally grown HgTe nanocrystals were first reported by Rogach et al. [34,35] with the synthesis being an extension of the previously published technique used for the preparation of cadmium chalcogenides [25,36,37]. The source of the mercury (II) ions is the perchlorate salt, which is dissolved in aqueous solution along with a 3-fold excess of 1-thioglycerol stabilizer. The pH is then adjusted to ~10 using 1 M $NaOH_{(aq)}$, and the mixture thoroughly de-oxygenated by N_2 bubbling. The H_2Te gas, generated by the action of dilute acid on aluminum telluride, is then injected into this N_2 flow, and subsequently dissolves in the alkaline mercury-thiolate solution to begin the nanocrystal growth process. High-resolution TEM (HRTEM) and X-ray diffraction measurements confirmed the presence of nanocrystalline HgTe in the bulk cubic coloradoite phase, with a broad size distribution of 3 to 8 nm, and an average diameter of 3.5 nm given by the Scherrer equation. Figure 7 shows the absorption and room-temperature PL spectra of a typical HgTe synthesis following the development of the nanoparticles over a period of 2 weeks.

All of the samples "age" at a progressively slower rate, pushing the PL and "excitonic" band-edge absorption peaks to longer wavelengths with time. After a period of 2 weeks, the PL has reached a wavelength of 1200 nm, and despite an apparent drop in intensity, the QE is still around 30%. In fact, the incredibly high QEs of around 50% for HgTe quantum dots is remarkable considering the surface is
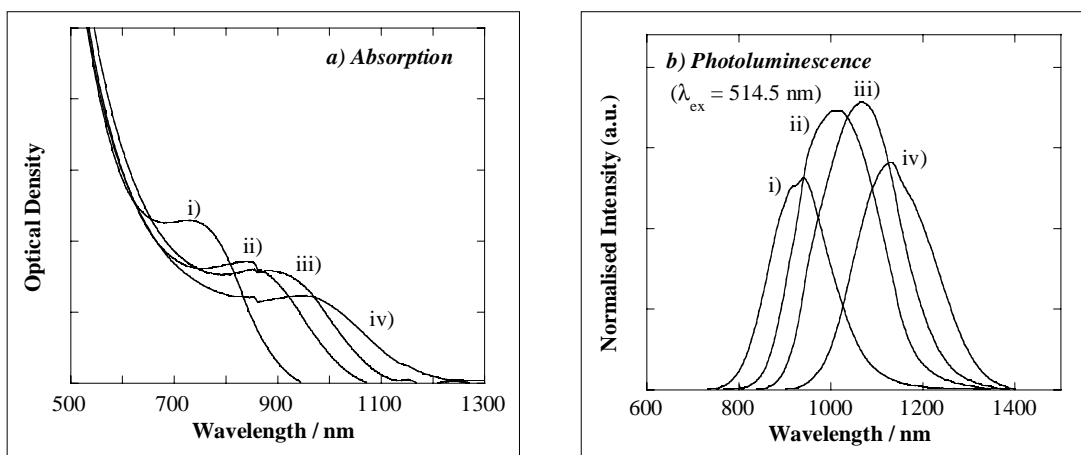

Fig. 7 (a) Absorption and (b) room temperature photoluminescence of HgTe recorded after (i) 60 min, (ii) 1 day, (iii) 3 days, and (iv) 2 weeks. Note that the Hg^{2+}:thiol:Te^{2-} ratio was 1:2.65:0.17.
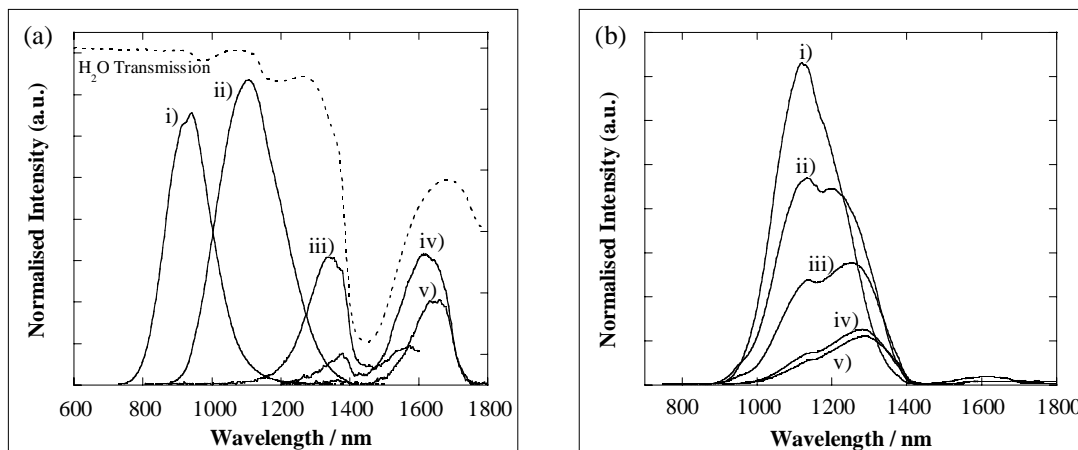
Fig. 8 The effect on the room temperature PL of nanocrystalline HgTe from (a) refluxing for (i) 0 min, (ii) 7 min, (iii) 12 min, (iv) 17 min, and (v) 22 min; and (b) varying the telluride quantity with a Hg^{2+}:thiol:Te^{2-} ratio of 1:2.6:*X* where *X* = (i) 0.17, (ii) 0.24, (iii) 0.44, (iv) 0.71, and (v) 1.24.

passivated only by an organic species. Previously, it has been thought that these kind of high QE values were only obtainable by inorganic-capped core-shell materials [28], and indicates that the thiol is providing extremely complete and efficient passivating layer. Following the initial dissolution of H_2Te, and the formation of the initial range of particle sizes, the system undergoes a shift towards larger diameters as the growth process continues. However, unlike the cadmium chalcogenides, it was not possible to reflux the solution to accelerate the ripening process without rapid loss of luminescence (see Fig. 8a). This was attributed to a thermal degradation of the thiol, with the labile R–S bond breaking, while the Hg–S bonding remained. HRTEM and EDAX studies confirmed the presence of sulfur in place of tellurium to a large extent within the refluxed nanocrystals. In fact, it is possible that this compositional redistribution is also responsible to the "normal" continuous room-temperature aging. Figure 8a also demonstrates nicely the difficulties of working with infrared-emitting materials in aqueous solution—the strong re-absorption of the PL by the solvent really obscures the spectral trends above about 1300 nm.

We have also investigated the effect on the optical properties of HgTe nanocrystals by varying the synthetic conditions [38]. It was found that the 1-thioglycerol content (above a critical value) and the pH (in the range 8 to 12) had little effect on the spectra, while the telluride content had a major effect. Figure 8b shows that increasing the Te^{2-} quantity results in longer wavelength PL (allowing for solvent re-absorption) giving a further degree of control over the emission wavelength.

While refluxing was found to kill the PL very quickly, gentle heating was effective in increasing the PL wavelength more into the telecoms region of interest [38]. Figure 9 shows the sequence of PL spectra for a sample heated at 70 °C for progressively longer times. In this case, the synthesis was performed using D_2O as solvent rather than ordinary water so that the strong IR absorptions did not obscure the luminescence spectra. Toward 1700 nm, the InGaAs detector begins to cut off, resulting in a distortion of the long wavelength sides of PL profiles (iii) and (iv)—the PL actually extends out to over 2000 nm. The integrated QE for curve (i) was about 40% when pumped in the visible, and does not decrease that dramatically as the PL shifts further into the infrared. Figure 9 really confirms the potential of this material for telecoms applications with the demonstration of strong luminescence covering the entire spectral region of interest—all the way from 900 to 2000 nm!
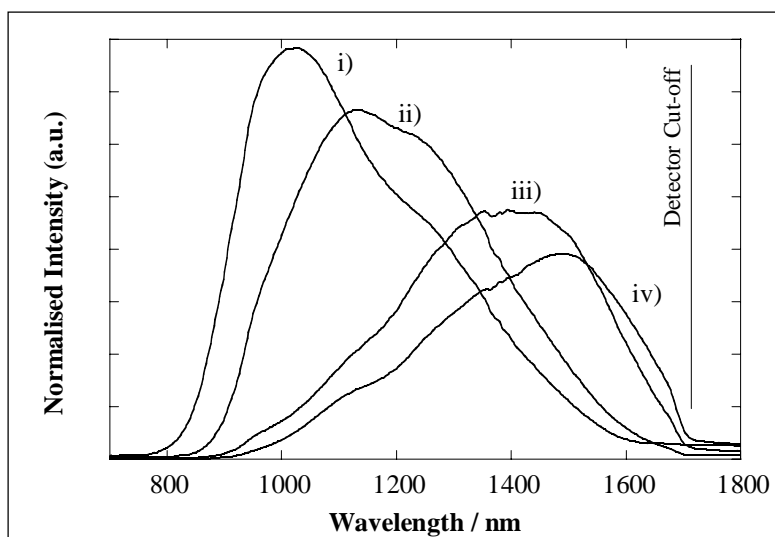
Fig. 9 Room-temperature PL spectra of HgTe preparation in D_2O following different amounts of heating under nitrogen at 70 °C after 1 day aging: (i) unheated, (ii) 30 min, (iii) 60 min, and (iv) 90 min.

CdS capping of HgTe nanocrystals

While we have managed to produce an extremely efficient infrared emitter in HgTe, this material is not without its problems. Its aging and sensitivity to heating are causes for concern, and, needless to say, for HgTe to be a useful material operating at the strategic near-infrared telecommunications wavelengths, the effect has to be eliminated. A possible way of achieving this is to cap the surface of the nanocrystals with a higher band-gap inorganic layer. These core-shell composite materials can increase the luminescence quantum yield due to improved passivation of the surface, and also tend to be more physically robust than the "bare" organically passivated clusters [28,39]. This should therefore produce
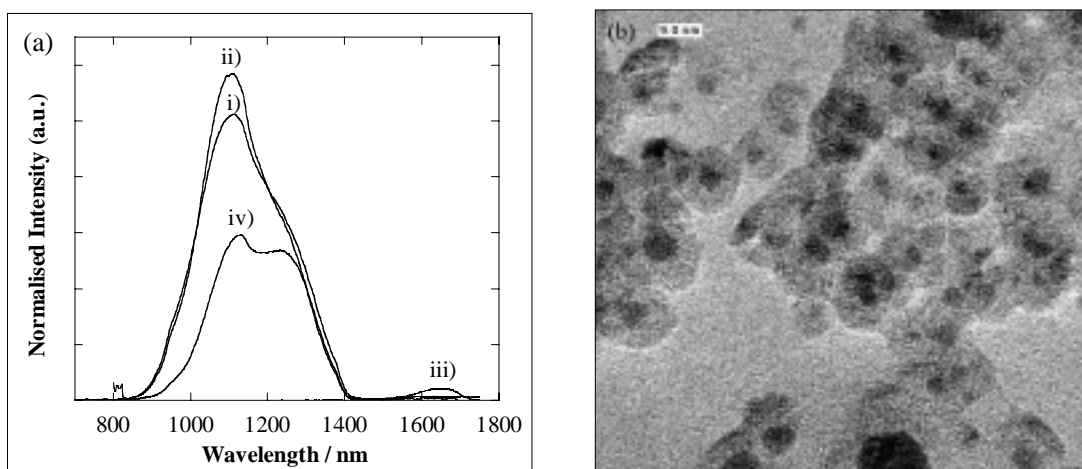

Fig. 10 Core-shell HgTe/CdS nanocrystals: (a) room-temperature photoluminescence spectra comparing (i) unheated bare HgTe, (ii) unheated HgTe/CdS, (iii) bare HgTe refluxed for 2 min, and (iv) HgTe/CdS refluxed for 30 min; (b) typical high-resolution TEM image of the 30-min refluxed HgTe/CdS sample.
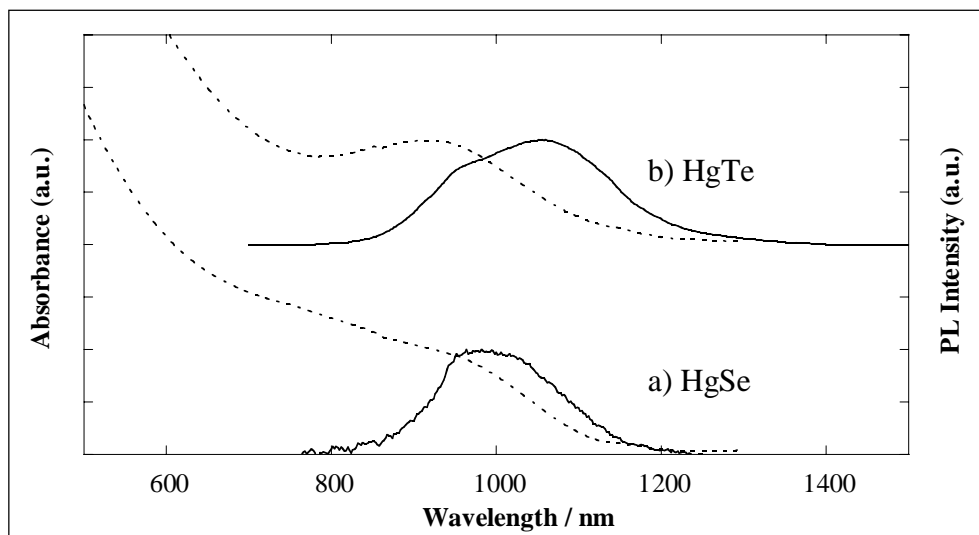
Fig. 11. Comparison of absorption (dashed line) and room-temperature PL (solid line) spectra for 1-day-old nanocrystalline (a) HgSe, and (b) HgTe.

a much more stable material where not only the aging process is suppressed, but which is more tolerant to the processing conditions necessary for incorporation into useful devices. Figure 10 shows the PL spectra and HRTEM image from HgTe/CdS core-shell nanocrystals, which were prepared by the standard aqueous technique, i.e., H_2S gas dissolving in an alkaline solution of as-prepared HgTe quantum dots with an excess of Cd^{2+} ions and 1-thioglycerol [40].

Core-shell structures can be clearly seen in Fig. 10b, with darker cores being surrounded by a lighter shell material. The inter-planar separations have been measured between 3.7 and 3.4 Å, which corresponds closely to the {111} lattice spacings of cubic coloradoite HgTe and cubic zinc blende CdS respectively. Plain HgTe and CdS nanocrystals are also present in the solution, but a large proportion of HgTe particles have definitely been over-coated with a thick (>2 nm) layer of CdS producing quite large composite structures from 5 to 10 nm in diameter.

The increased robustness of the CdS-capped material can be seen in Fig. 10a. Although there is a red-shift in the PL upon refluxing for 30 min, it is still strongly visible, unlike the bare particles which have virtually ceased luminescing after just a couple of minutes. In fact, the badly cut-off profile iv) represents a thermodynamically stable state for the HgTe/CdS composite, as neither prolonged refluxing or further aging has a pronounced effect on this luminescence, whereas the bare particles continue to red-shift. Note that there only is a small increase in QE upon introducing the outer shell, but this is not unexpected due to the already highly efficient process in the uncapped dots.

Other materials

Apart from CdTe and HgTe a number of other II-VI nanocrystals highlighted by Fig. 5 have been successfully prepared by the low-temperature aqueous/thiol route (e.g., HgSe, HgS, PbTe, and $Hg_xCd_{1-x}Te$ alloys) [41]. The complete description of the syntheses and optical properties of these alternative infrared materials is beyond the scope of this paper, but as an example of the versatility of this synthetic route, Fig. 11 shows the absorption and PL spectra after 1 day aging of HgSe quantum dots compared to HgTe.

The synthesis of nanocrystalline HgSe is exactly the same as for HgTe, with 1-thioglycerol used as stabilizer, except that Al_2Se_3 is used as the selenide source. It is useful to make the comparison with HgTe as bulk HgSe is also a semi-metal with a small negative bandgap and a cubic structure [33]. The physical behavior is similar, with HgSe aging gradually with time, and only being able to withstand very gentle heating. The optical properties are, however, quite different, with HgSe having a much lower QE (around 0.5%) and different absorption and PL profiles. HgSe has narrower but shorter wavelength PL, and the Stokes shift (i.e., the difference between PL and absorption peaks) is much smaller. Again, an inorganic capping layer of CdS improves the thermal robustness of the dots, as well as improving the QE several-fold to a few percent.

CONCLUSION

We have successfully demonstrated the potential of colloidally prepared semiconductor quantum dots for application as a true ultra-broadband optical amplifier in telecommunications systems operating both at the present and future low-loss fiber transmission windows. The burgeoning demand for bandwidth in the current exponential increase in network traffic is largely being met by WDM technologies, but improvements in amplifier performance are vital if this growth is to continue. A low-cost solution with a fully controllable gain profile would greatly increase the penetration of WDM into the telecommunications network. Mercury telluride quantum dots have been synthesized which have photoluminescence spectra that completely span the spectral region of interest, and give unequalled quantum efficiencies of tens of percent from 900 to over 2000 nm. The thermal robustness of this material has been significantly improved by the introduction of an inorganic CdS capping layer. This has important implications for the future application of the nanoparticles where post-processing will be required for device manufacture, and long-term optical stability will be vital. In addition to HgTe, many other infrared-emitting nanocrystals have been demonstrated to give as wide a range as possible of materials to build both simple and complex layered systems. Finally, some recent pump–probe measurements using liquid-filled capillary waveguides have indicated the possibility of infrared optical gain [41], further confirming the impact these materials may have on future optical networks.

References

1. P. Kaiser. IEEE/LEOS Summer Topicals - WDM Components, pp. 3–4, San Diego (1999).
2. D. A. Pinnow, T. C. Rich, F. W. Ostermayer, M. DiDomenico, Jr. *Appl. Phys. Lett*. **22**, 527–529 (1973).
3. S. Todoroki, S. Sakaguchi, K. Sugii, *Jpn. J. Appl. Phys. Pt. 1* **34**, 3128–3133 (1995).
4. O. Humbach, H. Fabian, U. Grzesik, U. Haken, W. Heitmann. *J. Non-Cryst. Solids* **203**, 19–26 (1996).
5. C. Forde and D. Tanis. Proceedings of NOC'99 - European Conference on Networks and Optical Communications, pp. 55–63, Delft, The Netherlands (1999).
6. P. W. France (ed.) 1st, Blackie & Son (1991).
7. E. Desurvire. *Erbium-Doped Amplifiers, Principles and Applications*, John Wiley & Sons, New York (1994).
8. M. Dejneka and B. Samson. *MRS Bulletin* **24**, 39–45 (1999).
9. Y. Sun, J. W. Sulhoff, A. K. Srivastava, J. L. Zyskind, T. A. Strasser, J. R. Pedrazzani, J. Wolf, J. Zhou, J. B. Judkins, R. P. Espindola et al. *Electron. Lett.* **33**, 1965–1966 (1997).
10. H. Masuda, S. Kawai, K. Aida. *Electron. Lett.* **34**, 567–568 (1998).

11. T. Shimada, Y. Nishida, K. Kobayashi, T. Kanamori, K. Oikawa, M. Yamade, Y. Ohishi, *Electron. Lett.* **33**, 1972–1973 (1997).
12. J. Kani and M. Jinno. *Electron. Lett.* **35**, 1004–1005 (1999).
13. S. V. Chernikov, Y. Zhu, R. Kashyap, J. R. Taylor. *Electron. Lett.* **32**, 2164–2165 (1996).
14. Y. Emori, K. Tanaka, S. Namiki. *Electron. Lett.* **35**, 1355–1356 (1999).
15. A. Galvanauskas, K. K. Wong, K. El Hadi, M. Hofer, M. E. Fermann, D. Harter, M. H. Chou, M. M. Fejer. *Electron. Lett.* **35**, 731–733 (1999).
16. A. L. Efros and A. L. Efros. *Sov. Phys. - Semicond.* **16**, 772 (1982).
17. A. I. Ekimov and A. A. Onuschchenko. *Sov. Phys. - Semicond.* **16**, 775 (1982).
18. R. Rossetti, S. Nakahara, L. E. Brus. *J. Phys. Chem.* **79**, 1086 (1983).
19. L. E. Brus. *J. Chem. Phys.* **80**, 4403–4409 (1984).
20. L. E. Brus and J. K. Trautman. *Phil. Trans. Roy. Soc. Lond. A* **353**, 313–321 (1995).
21. Y. Masumoto and K. Sonobe. *Phys. Rev. B* **56**, 9734–9737 (1997).
22. X. Peng, J. Wickham , A.P. Alivisatos. *J. Am. Chem. Soc.* **120**, 5343–5344 (1998).
23. C.B. Murray, D. J. Norris and M. G. Bawendi. *J. Am. Chem. Soc.* **115**, 8706–8715 (1993).
24. A. L. Rogach, L. Katsikas, A. Kornowski, D. Su, A. Eychmüller, H. Weller. *Ber. Bunsenges. Phys. Chem.* **100**, 1772–1778 (1996).
25. T. Vossmeyer, L. Katsikas, M. Giersig, I. G. Popovic, K. Diesner, A. Chemseddine, A. Eychmüller, H. Weller. *J. Phys. Chem.* **98**, 7665–7673 (1994).
26. W. Wang, Y. Geng, P. Yan, F. Liu, Y. Xie, Y. Qian. *J. Am. Chem. Soc.* **121**, 4062–4063 (1999).
27. T. Rajh, O. I. Micic, A. J. Nozik. *J. Phys. Chem.* **97**, 11999–12003 (1993).
28. M. A. Hines and P. Guyot-Sionnest. *J. Phys. Chem.* **100**, 468–471 (1996).
29. A. Eychmüller, A. Mews, H. Weller. *Chem. Phys. Lett.* **208**, 59–62 (1993).
30. A. A. Guzelian, U. Banin, A. V. Kadavanich, X. Peng, A. P. Alivisatos. *Appl. Phys. Lett.* **69**, 1432–1434 (1996).
31. S. V. Kershaw, M. Burt, M. Harrison, A. Rogach, H. Weller, A. Eychmüller. *Appl. Phys. Lett.* **75**, 1694–1696 (1999).
32. M. T. Harrison, S. V. Kershaw, M. G. Burt, A. Eychmüller, H. Weller, A. L. Rogach. *Mat. Sci. Eng. B* accepted for publication (1999).
33. I. Broser, H. Nelkowski, G. Nimitz. In *Semiconductors: Physics of II-VI and I-VII Compounds, Semimagnetic Semiconductors, Landolt-Bornstein: Numerical Data and Functional Relationships in Science and Technology*: New Series 17b, O. Madelung (ed.), pp. 244–252, Springer-Verlag, Berlin (1982).
34. M. T. Harrison, S. V. Kershaw, M. G. Burt, A. L. Rogach, A. Kornowski, A. Eychmüller, H. Weller. *MRS Symp. Proc.* **536**, 217–222 (1999).
35. A. L. Rogach, S. V. Kershaw, M. G. Burt, M. T. Harrison, A. Kornowski, A. Eychmüller, H. Weller. *Adv. Mater.* **11**, 552–555 (1999).
36. A. L. Rogach, L. Katsikas, A. Kornowski, D. Su, A. Eychmüller, H. Weller. *Ber. Bunsenges. Phys. Chem.* **101**, 1668–1671 (1997).
37. A. L. Rogach, A. Kornowski, M. Gao, A. Eychmuller, H. Weller. *J. Phys. Chem. B* **103**, 3065–3069 (1999).
38. M. T. Harrison, S. V. Kershaw, M. G. Burt, A. L. Rogach, A. Eychmüller, H. Weller. *J. Mater. Chem.* accepted for publication (1999).

39. B. O. Dabbousi, J. Rodriguez-Viejo, F. V. Mikulec, J. R. Heine, H. Mattoussi, R. Ober, K. F. Jensen, M. G. Bawendi. *J. Phys. Chem. B* **101**, 9463–9475 (1997).
40. M. T. Harrison, S. V. Kershaw, A. L. Rogach, A. Kornowski, A. Eychmüller, H. Weller. *Adv. Mater.* accepted for publication (1999).
41. S. V. Kershaw, M. T. Harrison, A. L. Rogach, A. Kornowski. *J. Sel. Top. Quant. Elec.: Nanostructures and Quantum Dots* submitted (1999).